VPI-8: A High-Silica Molecular Sieve with a Novel "Pinwheel" Building Unit and Its Implications for the Synthesis of Extra-Large Pore Molecular Sieves

Clemens C. Freyhardt,[†] Raul F. Lobo,[†,⊥] Shervin Khodabandeh,[†] John E. Lewis, Jr.,[†] Michael Tsapatsis,[†,||] Masahito Yoshikawa,[†] Miguel A. Camblor,[†,£] Ming Pan,[‡] Matthew M. Helmkamp,[†] Stacey I. Zones,[§] and Mark E. Davis*,[†]

Contribution from the Chemical Engineering, California Institute of Technology, Pasadena, California 91125, Center for Catalytic Science and Technology, Department of Chemical Engineering, University of Delaware, Newark, Delaware 19716, Gatan Inc., Pleasanton, California 94588, and Chevron Research and Technology Company, Richmond, California 97802

Received December 29, 1995[⊗]

Abstract: Relatively large (up to 4 μm), needle-like crystals of the high-silica molecular sieve VPI-8 are synthesized by hydrothermal methods and are subsequently calcined to remove the pore-filling organic TEA^+ (tetraethylammonium cation). Numerous physicochemical techniques are used to determine and characterize the structure of organic-free VPI-8. The structure is discussed with the use of two ordered topologies (**1a** and **1b**) and an average structure (**1c**) that accounts for the possibility of structural disorder in one of the T-atoms (Si1). The symmetry and space group of the ordered structure type **1a** (tetragonal, $P\bar{4}$ (no. 81)) is supported by electron diffraction data and the Rietveld refinement of the synchrotron X-ray powder data based on **1a** converges with the lowest agreement factors. The pore system of VPI-8 consists of one-dimensional channels containing 12-membered T-atom rings (12MRs) that run down the c-axis. HRTEM images along [001] confirm the general structure topology (the possible disorder occurs only along *c*). The structure of VPI-8 contains five unique T-atoms in atomic ratios of 1:4:4:4:4 per unit cell. These number densities are consistent with the data obtained from ^{29}Si solid-state NMR spectra. The main feature of the VPI-8 structure is a novel "pinwheel" framework building unit that has not been observed before in microporous materials and that seems well-suited for forming extra-large pore molecular sieves. Hypothetical framework models of extra-large pore molecular sieves containing one-dimensional 14MR (**2**), 16MR (**3**), 18MR (**4**), and 20MR (**5**) channel systems based on this new building unit are presented and discussed.

Introduction

Zeolites have found widespread use as adsorbents, ion exchangers, and catalysts. Zeolites with pores bounded by 8, 10 and 12 oxygen atoms (likewise 8, 10 and 12 silicon or aluminum atoms) are called small, medium, and large pore materials, respectively. Small, medium, and large pore zeolites have pore diameters of approximately 4.0, 5.5, and 7.5 Å, respectively, and each type of material is currently employed in large scale commercial applications. Most catalytic applications of zeolites have focused on medium and large pore materials. However, the recent trend is for catalytic applications of large pore zeolites with a desire for extra-large pore materials. Davis et al. proposed that materials with ring sizes above 12-membered rings (12MR) should be called extra-large pore materials.[1] To date, only phosphate-based molecular sieves like VPI-5 (contains 18MR) have extra-large pores.[2,3] Due to their low thermal stability and other factors,[4] the extra-large pore, phosphate-based molecular sieves have not found industrial applications. The need for extra-large pore zeolites (aluminosilicates) continues to be unfulfilled. Obvious applications for extra-large pore aluminosilicates range from catalytic cracking of large molecules to shape-selective catalysis on intermediates relevant to the pharmaceutical industries.

In this work, we present the solution and physicochemical characterization of the structure of the new zeolite VPI-8 (**1a**). The structure solution required the collaborative use of state-of-the art X-ray diffraction, high resolution transmission electron microscopy (HRTEM) and solid-state NMR techniques. The structure contains a heretofore unseen tertiary building unit ("pinwheel" building unit) that is capable of forming large and extra-large pore frameworks. In addition to VPI-8, hypothetical extra-large pore frameworks are illustrated to show the generality of using the new atomic arrangement to provide models for highly desired, novel materials.

Experimental Section

Synthesis. Several methods to prepare VPI-8 have been reported.[5−7] However, all the previous procedures have given VPI-8 with small crystal size (<1 μm) and thus provide X-ray diffraction data of

* To whom correspondence should be addressed.
[†] California Institute of Technology.
[‡] Gatan, Inc.
[§] Chevron Research and Technology Company.
[⊥] University of Delaware.
[||] Current address: University of Massachusetts, Amherst, MA 01003.
[£] Current address: Instituto de Tecnologia Quimica, Valencia, Spain.
[⊗] Abstract published in *Advance ACS Abstracts,* July 15, 1996.

(1) Davis, M. E.; Hathaway, P. E.; Montes, C. *Zeolites* **1989**, *9*, 436−439.
(2) Davis, M. E.; Saldarriaga, C.; Montes, C.; Garces, J. M.; Crowder, C. A. *Nature* **1988**, *331*, 698−699.
(3) Davis, M. E.; Montes, C.; Hathaway, P. E.; Arhancet, J. P.; Hasha, D. L.; Garces, J. M. *J. Am. Chem. Soc.* **1989**, *111*, 3919−3924.
(4) Davis, M. E.; *Chem. Ind*. (London) 1992, 137−139.
(5) Annen, M. J. Ph.D. Thesis, Virginia Polytechnic Institute and State University, 1991.
(6) Annen, M. J.; Davis, M. E. *Microporous Mater.* **1993**, *1*, 57−65.

insufficient quality for use in Rietveld refinement due to particle size line broadening. Here, a method to prepare larger crystals is provided. This procedure produced crystals of size sufficient to give high quality powder X-ray diffraction data. The synthesis of the larger, i.e., up to 4 μm, high-quality crystals of VPI-8 required the use of seed crystals. The seed crystals were synthesized from a reaction mixture of molar composition $1SiO_2$:$0.1Zn(CH_3COO)_2 \cdot 2H_2O$:$0.2LiOH$:$0.4TEAOH$:$30H_2O$. In a typical preparation, 0.67 g of LiOH (Fisher) were dissolved in a solution obtained by combining 20.74 g of a 40% aqueous solution of tetraethylammoniumhydroxide (TEAOH, Johnson Matthey) and 54.40 g of distilled water. After the LiOH was completely dissolved, 3.09 g of $Zn(CH_3COO)_2 \cdot 2\ H_2O$ (Fisher) were added, and the solution was stirred for 1 h. With stirring, 21.10 g of colloidal SiO_2 (Ludox HS-40) were added, and the agitation was continued for 2 h. The reaction mixture was then charged into a 125 mL Teflon-lined stainless steel autoclave (Parr) and allowed to react under autogenous pressure for 14 days at 423 K. The resulting product was recovered by vacuum filtration, washed with distilled water, and dried in air at room temperature. The recovered solid obtained from this synthesis procedure was then analyzed for phase purity and crystallinity using powder X-ray diffraction (described below).

The larger crystals of VPI-8 used for the structure determination were synthesized using the seed crystals prepared as described above. A starting mixture with a molar composition of $1SiO_2$:$0.036Zn(CH_3COO)_2 \cdot 2H_2O$:$0.26NaOH$:$0.78TEAOH$:$21H_2O$ was formulated as follows. NaOH (0.19 g, 97%, EM) and 0.14 g of $Zn(CH_3COO)_2 \cdot 2H_2O$ were dissolved in a solution obtained by combining 5.0 g of TEAOH (40% aqueous solution, Aldrich) and 2.34 g of distilled water. After stirring this solution for 30 min, 2.61 g of colloidal SiO_2 (Ludox HS-40) were added. With continuous agitation, 0.040 g of the seed crystals was added, and the total mixture was stirred overnight at room temperature. The reaction mixture was charged into a 25 mL Teflon-lined stainless steel autoclave (Parr) and heated under autogenous pressure for 10 days at 423 K. The product was collected by vacuum filtration, washed with distilled water, and dried in air at room temperature. To remove the occluded organic molecules, the sample was heated in air to 823 K within 5 h and maintained at this temperature for 3 h. After calcination, the material used for collecting the synchrotron powder X-ray diffraction data (vide infra) was treated with aqueous NH_4Cl solution as follows. The calcined larger crystal VPI-8 (0.25 g) was combined with 250 mL of 0.1 M aqueous NH_4Cl solution and heated at 353 K for 2 h. The treated crystals were recovered by vacuum filtration and washed with distilled water. This procedure, i.e., treatment with NH_4Cl solution, recovery by filtration, and washing was repeated three times to remove residual amorphous materials remaining from the synthesis from the VPI-8 crystals. Finally, the material was dried in air at room temperature.

In order to assist the study of VPI-8 by ^{29}Si MAS−NMR, Fe^{3+} containing VPI-8 samples ($VPI\text{-}8_{Fe}$) were prepared (Fe^{3+} was used here as a paramagnetic relaxing agent for silicon). The Fe^{3+} containing material was prepared by the same method as the larger crystals of VPI-8 except $Fe(NO_3)_3 \cdot 9\ H_2O$ was used as a source of Fe. $VPI\text{-}8_{Fe,1}$ was prepared by adding 0.014 g of $Fe(NO_3)_3 \cdot 9\ H_2O$ after the addition of NaOH to the initial solution during preparation of the synthesis gel [$(Si/Fe)_{gel} = 500$]. Similarly, $VPI\text{-}8_{Fe,2}$ was prepared by adding 0.007 g of $Fe(NO_3)_3 \cdot 9\ H_2O$ after the addition of NaOH to the initial solution during the preparation of the synthesis gel [$(Si/Fe)_{gel} = 1000$]. The VPI-8 crystals used for ^{1}H-^{29}Si CP MAS measurements were prepared in the following manner: 0.39 g of calcined larger crystal VPI-8 was stirred in 100 mL of 0.01 M aqueous HCl solution overnight at room temperature, recovered by vacuum filtration, washed with distilled water, and dried in air at room temperature. The dried material was heated at 523 K under vacuum for 2 h and then contacted with cyclohexane vapors at a pressure of 25 mmHg for 1 h at room temperature.

Elemental Analysis. Silicon and zinc analyses were performed by Galbraith Laboratories, Inc. (Knoxville, TN).

Thermogravimetric Analysis (TGA). Standard TGA measurements were carried out on a Du Pont 951 thermogravimetric analyzer in flowing, dry argon using a constant heating rate of 1 K/min from 298 to 1173 K.

Scanning Electron Microscopy (SEM). SEM images were recorded on a Camscan 2-LV scanning electron microscope operating with an accelerating voltage of 15 kV.

X-ray Diffraction Analysis. Room temperature powder X-ray diffraction (PXRD) patterns were recorded on a Scintag XDS 2000 diffractometer (liquid nitrogen cooled germanium detector, Cu Kα radiation, $\lambda = 1.54184$ Å) with a Bragg-Brentano geometry. Room temperature synchrotron powder X-ray diffraction (SPXRD) patterns ($\lambda = 1.30800$ Å) were collected at the National Synchrotron Light Source, Beam Line X7A in Brookhaven, New York. To remove any physisorbed water from the micropores the sample-holder containing the well-ground sample was evacuated, heated at 200 °C for 2 h, and sealed under vacuum.

MAS−NMR. Solid-state NMR spectroscopy was performed using a Bruker AM 300 spectrometer equipped with a high power assembly for solids. Samples were packed into 7 mm ZrO_2 rotors and spun in air. ^{29}Si (59.63 MHz) spectra were obtained using magic angle spinning (MAS) at spinning rates of 3.7 kHz, pulse widths of 4 μs (40° pulse), and recycle delays of 10−300 s. ^{1}H−^{29}Si CP/MAS spectra were measured with ^{1}H decoupling at spinning rates of 2.5−3 kHz using a 7 μs ^{1}H pulse (^{1}H 90°), ^{29}Si contact times of 0.3−50 ms, and recycle times of 5 s. Tetrakis(trimethylsilyl)silane was used as the reference material for ^{29}Si chemical shift determinations, and all chemical shifts are reported in ppm relative to external TMS. Exponential line-broadening of 10−30 Hz was applied to the data and spectral fitting was performed using both the Bruker LINESIM and the QNMR software packages.

Fourier Transform Infrared Spectroscopy (FTIR). Infrared spectra were obtained using a Nicolet System 800 Spectrometer (KBr beamsplitter and MCT-A detector) with self-supporting pellets of calcined and acid washed VPI-8. A heated sample cell which was continuously purged with dry argon gas was used to collect spectra under anhydrous conditions at elevated temperatures.

High Resolution Transmission Electron Microscopy (HRTEM). The samples for HRTEM were prepared by embedding the crystals in epoxy and microtoming. HRTEM was performed on a JEOL JEM 4000EX electron microscope operated at 400 kV (point resolution 1.7 Å) with a Gatan 679 slow-scan CCD (charge-coupled device) camera. The CCD camera has 1024 × 1024 pixels, and each pixel is 24 × 24 μm^2. A low-dose imaging technique was used to minimize beam damage to the sample.[8] A real-space averaging technique was used to suppress image noise and bring out high-resolution structure information.[8]

Single-Crystal Electron Diffraction (ED). Selected area ED images were collected using a Philips 430 electron microscope operating at 200 kV. Tilting experiments of single crystallites were performed in a tilt rotation holder.

Computer Simulations. Initial distance least squares (DLS) refinements using the program system DLS-76,[9] PXRD simulations, and multislice HRTEM simulations were performed on a Iris workstation using the commercially available Cerius software package.[10] Rietveld refinement of the SPXRD data was accomplished using the General Structure Analysis System (GSAS).[11]

Results and Discussion

Approaches to the Structure Solution of VPI-8. Solution of the VPI-8 structure required the collaborative use of numerous techniques in order to correctly deduce the topology. Physicochemical data published previously established the existence of a one-dimensional large pore system in the structure (at least 12MRs with free pore diameter above 6 Å, by TEM and cyclohexane adsorption data) and a framework density (FD) of approximately 18 T-atoms per 1000 Å^3 (pycnometry used to

(7) Camblor, M. A.; Yoshikawa, M.; Zones, S. I.; Davis, M. E. In *Synthesis of Microporous Materials: Zeolites, Clays, Nanocomposites*; Occelli, M., Kessler, H., Eds.; Marcel Dekker: New York, in press.

(8) Pan, M.; Crozier, P. A. *Ultramicroscopy* **1993**, *48*, 322−340.

(9) Baerlocher, C.; Hepp, A.; Meier, W. M. *Distance Least Squares Refinement Program DLS-76*, ETH, Zurich, 1977.

(10) *Cerius Version 3.2*; Molecular Simulations: Cambridge, UK.

(11) Larson, A. C.; Von Dreele, R. B. *General Structure Analysis System GSAS*; Los Alamos National Laboratory: Los Alomos, NM, 1994.

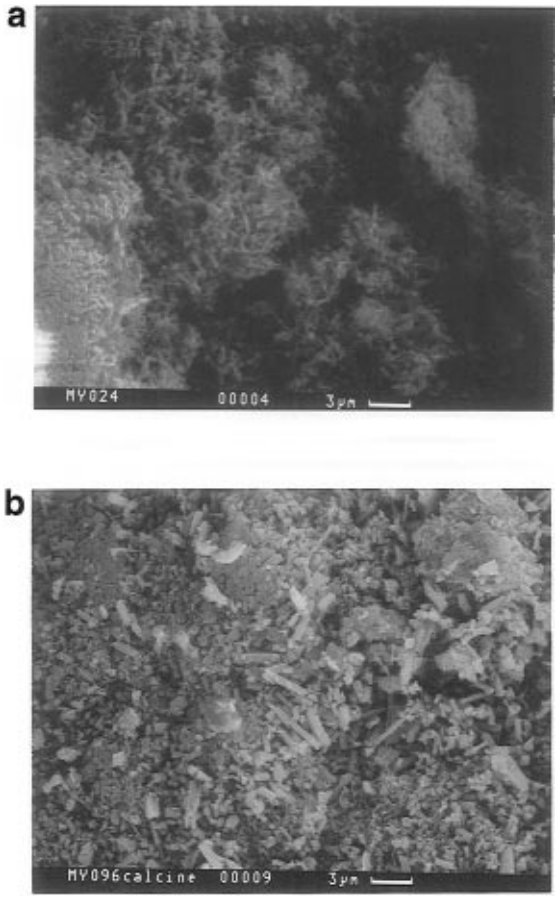

Figure 1. SEM images showing morphologies and crystal sizes for (a) calcined VPI-8 seed crystals (<1 μm) and (b) larger calcined VPI-8 crystals (up to 4 μm) used for structure determination.

give density) that corresponds to 16 T-sites per unit cell.[7] In the present work, the physical adsorption of 2,2-dimethylpropane ($P/P_o = 0.20$, 298 K) on the larger crystals gives an uptake of 0.04 cm^3/g confirming previous results on the small-crystal VPI-8 and indicating the presence of micropores in the structure with free diameters of about 6.2 Å, i.e., the reported kinetic diameter of 2,2-dimethylpropane.[12]

Figure 1 shows the morphologies and sizes of the two different VPI-8 samples. The unseeded synthesis of VPI-8 leads to a material that mainly contains submicron crystallites (Figure 1a). Using these small crystals as seeds in a further synthesis, a VPI-8 sample with larger, up to 4 μm sized crystals are obtained (Figure 1b). Comparison of the PXRD diagrams of the calcined form of these two VPI-8 samples (Figure 2) shows the large-crystal material to have a higher crystallinity and thus provide a better resolution, especially for the numerous weak reflections in the high 2θ-range of the PXRD patterns. Therefore, a calcined, large-crystal VPI-8 sample was used for collecting the SPXRD data shown in Figure 3. Indexing the SPXRD pattern leads to a tetragonal unit cell with cell parameters of $a = b = 13.053$ Å and 5.037 Å (cf. Table 1). It has been shown previously that the unit cell parameters are approximately $a = b = 13.1$ Å and $c = 5.1$ Å but vary with zinc content as expected.[7] However, chemical analysis of the seeded synthesis product (ratio Si:Zn > 2000) shows that the large-crystal VPI-8 sample used for SPXRD is essentially a pure SiO_2 phase. In the course of solving the structure of VPI-8, over 30 different models were built. Their simulated PXRD patterns were compared to the experimental PXRD diagram but

(12) Breck, D. W. *Zeolite Molecular Sieves*; Robert E. Krieger: Florida, 1984; p 636.

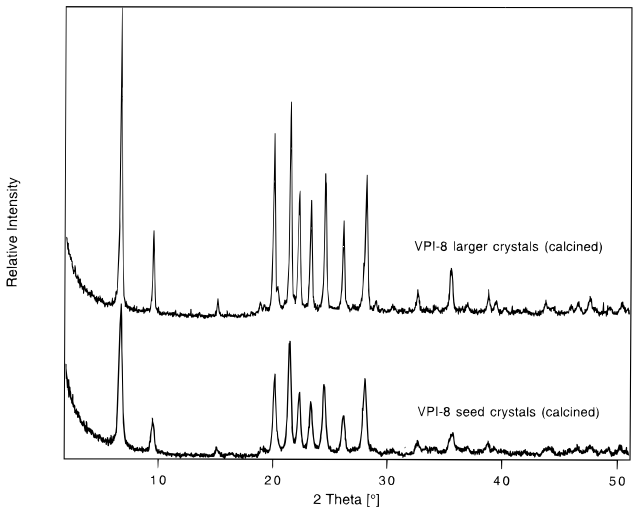

Figure 2. Comparison of powder X-ray diffraction data for calcined VPI-8 seed crystals (<1 μm) and larger calcined VPI-8 crystals (up to 4 μm) used for structure determination.

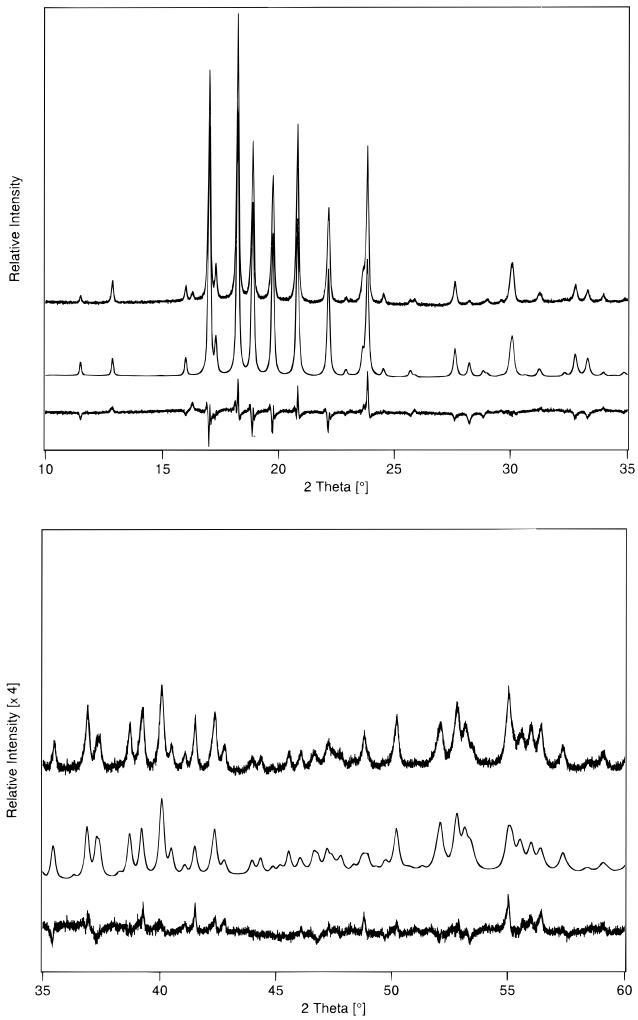

Figure 3. Observed (upper), calculated (middle) and difference (lower) profiles for SPXRD patterns of VPI-8 ($\lambda = 1.308\,00$ Å). The relative intensity scale has been increased by a factor of four for the section spanning 35−60 °2θ.

did not lead to a satisfactory match of both data. Additional attempts to apply direct methods to solve the structure of VPI-8, using 70 of the observed reflections in the SPXRD pattern, failed to yield the precise topology but, however, did give some indications for probable atomic positions.

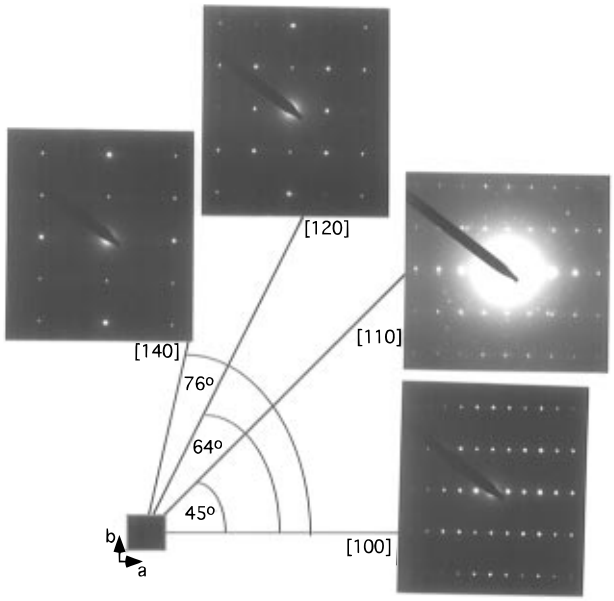

Figure 4. Single-crystal electron diffraction patterns collected along [*hk*0] zone axes. Experimentally determined tilt angles between indicated zone axes are shown on the schematic single-crystal.

Next, extensive HRTEM investigations were employed, as they are a very powerful tool in determining ring or pore sizes of zeolite structures with one-dimensional (1D) pore systems in general and solving the VPI-8 structure in particular. Single-crystal electron diffraction (ED) studies showed the selected, individual crystals of the calcined, large-crystal VPI-8 sample to be free of twinning and faulting (Figure 4). This is discerned by the fact that no streaking or doublets in the electron diffraction spot patterns are observed. Single-crystal tilt ED experiments confirmed the tetragonal symmetry of the VPI-8 structure and yielded unit cell parameters consistent with those obtained from the X-ray data. HRTEM images (Figures 5a,b) recorded along the [00$\bar{1}$] zone axis, i.e., the long axis of the needle-shaped VPI-8 crystals, revealed the existence of large, 1D channels (containing 12MRs or larger) running parallel to *c*. These large channels are separated by walls (comprised of 5MRs and 6MRs) containing pairs of two smaller pores alternating with a group of four equal-sized small-ring pores arranged in a pinwheel configuration (Figure 5b). Understanding this four-hole pinwheel pattern turned out to be the key for unlocking the structure of VPI-8.

The topology of the structure shown in Figures 5−8 was finally obtained by an iterative process of model building, distance least squares refinement (DLS)[9] of the model-derived atom positions, computer simulation (CERIUS)[10] of the corresponding PXRD patterns and HRTEM images, and subsequent comparison to the experimental SPXRD and HRTEM data.

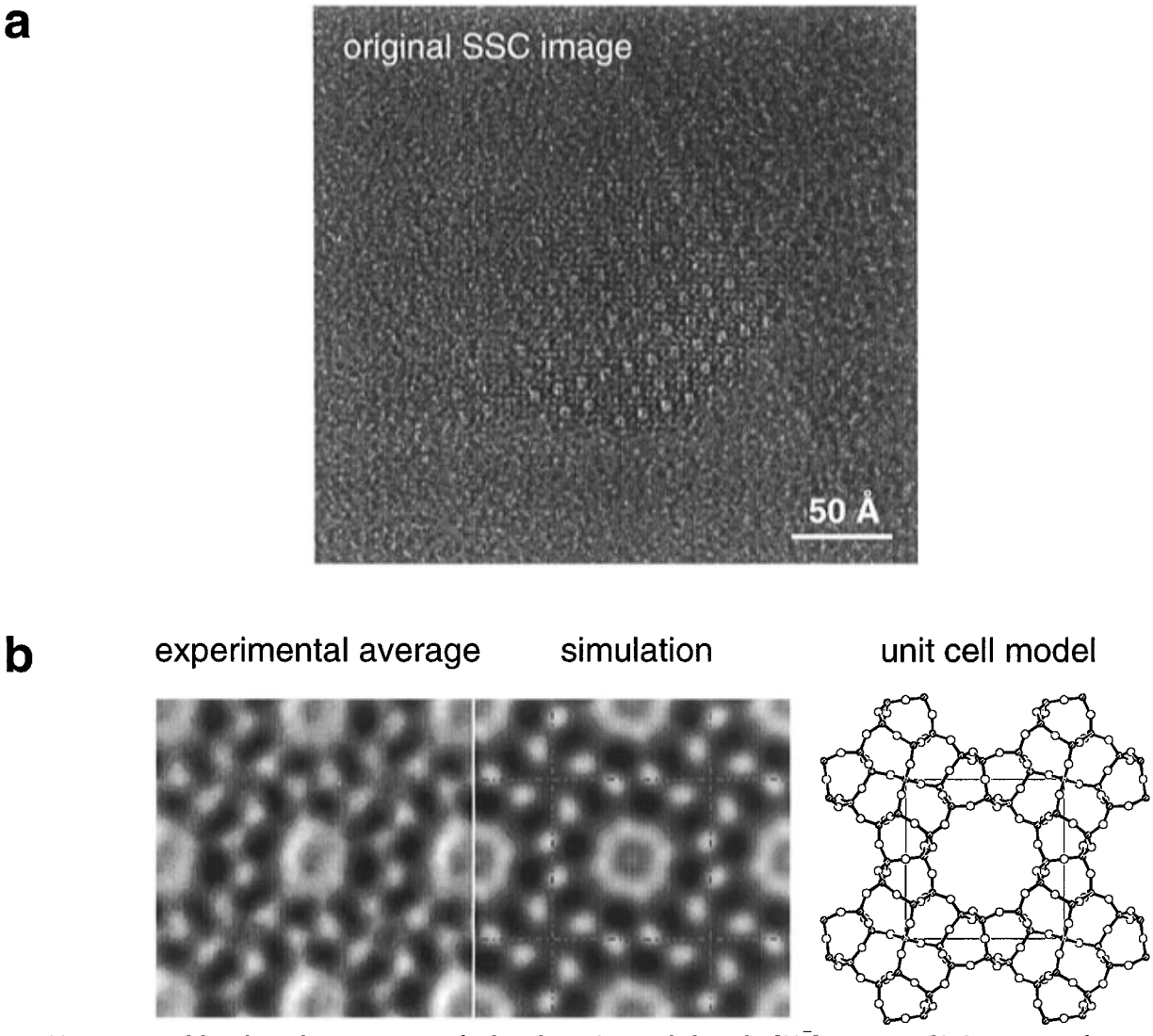

Figure 5. (a) Experimental low-dose, slow-scan image of calcined VPI-8 viewed along the [00$\bar{1}$] zone axis. (b) Comparison of experimental real-space averaged, simulated, and atomic model images.

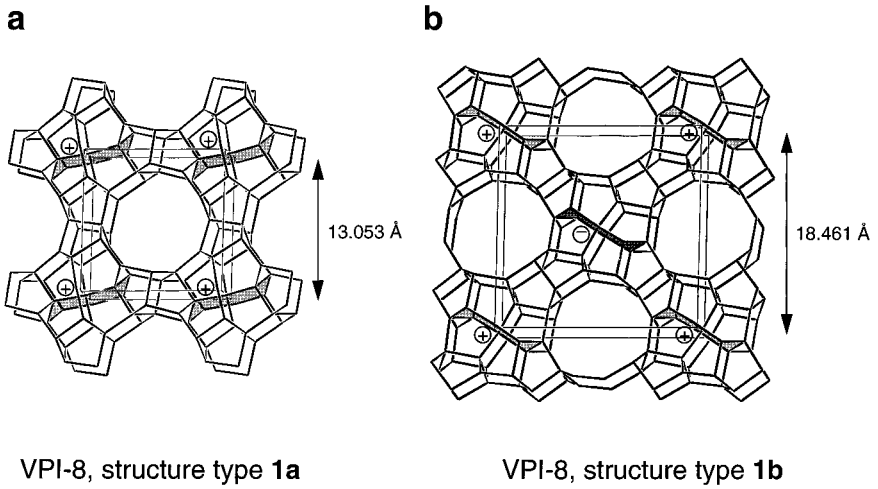

Figure 6. Topology of the two possible, closely related structure types for VPI-8. (a) VPI-8 (**1a**) with $a = b = 13.053$ Å, $c = 5.037$ Å (space group $P\bar{4}$). (b) Structure type **1b** with with $a = b = 18.461$ Å, $c = 5.038$ Å (space group $P4_2/n$). Some heart-shaped 8MRs in the center of the new pinwheel structure building unit (see Figure 7) are shaded; relative orientation (up and down pointing) of the 8MR hearts is symbolized by + and − signs, respectively.

Following this procedure, a tetragonal structure topology based on a new pinwheel building unit was obtained (Figure 6). However, during the course of model building it was recognized that there are possible variations of this topology, with only minor changes in the overall structure connectivity. From a stereochemical point of view, no obvious reason could be seen for preferring one topology over the other. It was brought to our attention that these variations can be crystallographically described as a slight disorder within the structure. Since the HRTEM images along the large pores do not indicate any faulting perpendicular to the pores (see Figure 5), the disorder has to occur along the pores. It is also clear from HRTEM that all explored models need to have the same *a*,*b*-projection, in order to keep the same arrangement of small and large pores. Following these premises, all obtained structure models turn out to have five crystallographically inequivalent T-atoms; four (T2, T3, T4, T5) form the general tetragonal pinwheel topology of VPI-8, and one T-atom (T1) is located at the center of the pinwheel. The pinwheels contain four 5MRs in a square-like arrangement, and each 5MR shares three T-atoms (T1, 2 × T2) with two adjacent 5MRs. Translational symmetry along c causes the formation of infinite one-dimensional pinwheel columns. These pinwheel columns are connected via pairs of additional 5MRs to form a square-like arrangement of columns producing the large 12MR channels. Keeping the positions of T2, T3, T4, and T5 fixed, there are two possibilities to place T1 in the center of the pinwheel with respect to its *z*-coordinate. Having T1 at 0,0,1/2 (Si1a) leads to a tetrahedral coordination of T1 by four symmetrically equivalent T2 atoms located at either $z = 1/4$ or $z = 3/4$. Placing T1 at 0,0,0 (Si1b) results in a slightly different tetrahedral arrangement of four T2 ($z = -1/4$ or 1/4) around T1. Exclusive occupation of either position Si1a or Si1b in each pinwheel unit leads to the primitive tetragonal, acentric topology of VPI-8 (**1a**), with maximum topological space group symmetry $P\bar{4}$ (no. 81) and unit cell dimensions of $a_1 = b_1 \approx 13$ Å and $c_1 \approx 5$ Å (Figure 6a). Alternating occupation of T-site Si1a and Si1b in every second pinwheel column produces a centrosymmetric, pseudo-I-centered lattice (**1b**) with maximum topological symmetry $P4_2/n$ (no. 86) and $a_2 = b_2 = \sqrt{2}\cdot a_1 = \sqrt{2}\cdot b_1 \approx 18.5$ Å and $c_2 = c_1 \approx 5$ Å, resulting in a doubling of the unit cell volume (Figure 6b). Both ordered structure topologies **1a** and **1b** were investigated by Rietveld refinement using the experimental SPXRD data (see below). In order to account for the possibility of completely random distribution of occupied Si1a and Si1b sites, a third, disordered model for VPI-8 (**1c**) was also studied. The disorder was modeled by placing Si-atoms with site occupancy factor (sof) of 0.5 at both T1-sites in the structure models of **1a** and **1b** (corresponds to a split T1 position in both topologies). Here, only the disordered model of **1a** is discussed, since the results for both Rietveld refinements lead to almost identical structural parameters. Thus, **1c** can also be regarded as a superimposed or averaged structure of **1a** and **1b**.

Rietveld Refinement of VPI-8. Three different structural models of VPI-8 were investigated using the Rietveld method. In addition to the ordered models **1a** ($P\bar{4}$) and **1b** ($P4_2/n$), a completely disordered model (**1c**, $P\bar{4}$) with respect to the T1 position was also studied. As indicated above, the main difference between structure type **1a** and **1b** is the relative position of the T1 atoms in the center of the pinwheel unit. Within each pinwheel column, the T1 positions in both structure types are separated by one repeat unit along *c* (∼5 Å). Between different pinwheel columns in **1a**, the T1 (Si1a) atoms are related to one another by translations of ∼13 Å along $\pm a_1$ or $\pm b_1$, i.e., the directions of the basis vectors in the $P\bar{4}$ unit cell (see Figure 6a). In contrast, the T1 (Si1b) atoms in the $P4_2/n$ model **1b** are related by translations of ∼13 Å along $\pm(a_2 + b_2)$ or $\pm(a_2 - b_2)$ (corresponding to directions $\pm a_1$ or $\pm b_1$ in **1a**) plus a shift of 1/2 (∼2.5 Å) along $\pm c_2$. In the disordered model **1c** each of the T1-sites Si1a and Si1b possess the same symmetry relationship as T1 in **1a**.

The initial atomic positions for the Rietveld refinements were taken from the results of DLS optimization of the two ordered structure models **1a** and **1b**. As mentioned above, the disorder in **1c** was modeled by using split atom positions for T1 (Si1a, Si1b) and O12 (O12a, O12b). Only silicon atoms were used to occupy the T-atom positions, since chemical analyses showed only a small amount of zinc (∼0.05 wt%) in the sample. Details of data collection, final refinement results, and crystallographic data for all three models are listed in Table 1.

Refinement of Ordered Structure Type 1a. First, background and scale factors were refined (10−60 °2θ) using a fixed background subtraction based on eight data points plus a cosine Fourier series function with a total of six parameters. After obtaining a good background fit, the unit cell parameters and profile coefficients[11,13] were refined and followed by the refinement of the zero point correction. For the refinement of atomic parameters, soft geometric constraints for Si−O bond

Table 1. Crystallographic Data, Details of Data Collection and Rietveld Refinement for Ordered Structure Types **1a** and **1b** and Disordered Structure Type **1c** of Calcined VPI-8

	1a	**1b**	**1c**
chemical formula	$[Si_{17}O_{34}]$	$[Si_{34}O_{68}]$	$[Si_{17}O_{34}]$
formula weight	1021.53	2043.06	1021.53
crystal system	tetragonal	tetragonal	tetragonal
space group (no.); *Z*	$P\bar{4}$ (81); 1	$P4_2/n$ (86); 1	$P\bar{4}$ (81); 1
cell parameters			
a, *b* [Å]	13.0527(5)	18.4607(6)	13.0528(5)
c [Å]	5.0373(2)	5.0377(2)	5.0374(2)
unit cell volume [Å^3]	858.23(6)	1716.84(11)	858.24(6)
calculated density [g/cm^3]	1.976	1.976	1.976
framework density [T/1000 Å^3]	19.8	19.8	19.8
data collection temp [K]	298	298	298
wavelength [Å]	1.30800	1.30800	1.30800
2θ range [deg]	10−60	10−60	10−60
step scan increment [deg]	0.005	0.005	0.005
no. of obsvns	10000	10000	10000
no. of contributing reflcns	398	398	398
no. of structural parameters	41	44	40
no. of profile parameters	10	10	10
R_p	0.083	0.089	0.084
R_{wp}	0.105	0.112	0.109

distances [d(Si−O) = 1.60 Å] and interatomic O−O distances [d(O−O) = 2.61 Å] were used at all times. Consecutive refinement of the isotropic displacement parameters (U_{iso}, refined jointly for each atom type) of the Si and O atoms converged at the final stage to residual values of $R_p = 0.083$ and $R_{wp} = 0.105$, respectively. Relaxation of the soft constraints improved the residuals but unreasonable Si−O bond distances and interatomic angles were obtained. The experimental, calculated, and difference PXRD patterns for the Rietveld refinement based on the ordered structure type **1a** are shown in Figure 3. Final atomic parameters and selected interatomic distances and angles for **1a** are given in the supporting information. Corresponding tables for the Rietveld refinements of **1b** and **1c** together with the XRD powder graphs (experimental, calculated, and difference diagram, cf. Figure 3) are also provided as supporting information. The Si−O bond distances for **1a** are in the range of d(Si−O) = 1.535(3)−1.645(3) Å with an average value of $\bar{d}$(Si−O) = 1.597 Å. The O−Si−O angles are between 91.5 and 124.2° [$\bar{\angle}$(O−Si−O) = 109.0°] and the Si−O−Si angles range from 137.4 to 173.1° [$\bar{\angle}$(Si−O−Si) = 154.1°]. Although these values are within the expected ranges reported for Rietveld refinements of zeolites,[14] it is obvious from Figure 3 that the fit of experimental and calculated PXRD data still shows some discrepancies. Some of the discrepancies between the calculated and experimental XRD patterns are certainly due to the fact that VPI-8 contains silanol groups from the hydrolysis of T1-O-T2 linkages (see NMR, IR, and TGA data below) that cannot be accounted for in the refinement process. This shortcoming can not be overcome and must be considered when evaluating refinement residuals and bond distances and angles involving T1 and T2.

Refinement of Ordered Structure Type 1b. From analysis of the systematic absences in the experimentally obtained SPXRD pattern of VPI-8, it was not possible to discriminate between the space groups $P\bar{4}$ and $P4_2/n$ of the ordered structure types **1a** and **1b**, respectively. Since the 001 reflection is not observed, and the presence of the 003 reflection cannot be confirmed due to other overlapping reflections, it is arguably possible that the space group of VPI-8 could contain a 4_2 screw axis along *c*, i.e., support of model **1b**. However, ED images recorded along the [$\bar{1}$00] zone axis are in disagreement with this postulate (see Figure 4). Within the selected area of the ED pattern, no systematic absences can be observed along *c**. To further investigate this issue, a Rietveld refinement based on structure type **1b** was carried out following the same procedure that was used for **1a**. For the refinement of **1b**, the default origin choice 2 (origin located at $\bar{1}$) in GSAS was used. The final residual values ($R_p = 0.089$, $R_{wp} = 0.112$) were only slightly higher than the respective values obtained for **1a**. However, close inspection of the final XRD difference pattern indicates that several reflections in the calculated XRD pattern are not observed in the experimental SPXRD data. The Si−O bond distances for **1b** are in the range of d(Si−O) = 1.41(1) − 1.677(9) Å with an average value of $\bar{d}$(Si−O) = 1.599 Å. The O−Si−O angles range from 91.9° to 133.6° [$\bar{\angle}$(O−Si−O) = 108.7°, while the Si−O−Si angles are between 131.4(9) and 180.0° [$\bar{\angle}$(Si−O−Si) = 155.0°]. Most interatomic distances and angles for **1b** are in reasonable ranges, but they differ somewhat from the values obtained for **1a**. Despite the geometric constraints imposed on the model, the distance between Si5 and O45 consistently converged to a value of d(Si5−O45) = 1.41 Å in final refinement cycles. Additionally, one T−O−T angle, namely ∠(Si5−O55−Si5), appears to be 180° by symmetry (caused by the location of O55 on an inversion center ($\bar{1}$) at 1/2,0,1/2). Recent work on the structure of highly siliceous ferrierite[15,16] strongly suggest that the presence of T−O−T angles of 180° are very unlikely. These results in combination with the ED data suggest that structure type **1b** is not the correct description for VPI-8.

Refinement of the Disordered Structure Type 1c. For the starting model of **1c**, the atom position of T1 (Si1a) in **1a**, located at 0,0,1/2, was split into two positions; Si1a at 0,0,1/2 and Si1b at 0,0,0 with sof = 0.5 in each case (all parameters kept fix). The disorder of T1 also implies a disorder in the location of O12. For this reason O12 of **1a** was similarly split into two oxygen atoms (sof = 0.5), specified as O12a (bonded to T-atoms Si1a and Si2) and O12b (bonded to T-atoms Si1b and Si2). During refinements the *x*,*y*,*z*-coordinates of these two oxygen atoms were constrained such that

$$x(\mathrm{O12a}) = x(\mathrm{O12b})$$

$$y(\mathrm{O12a}) = y(\mathrm{O12b})$$

$$z(\mathrm{O12a}) = 0.5 - z(\mathrm{O12b})$$

and the position of Si2 was fixed along the c-direction with $z = 0.75$. Besides these differences, the Rietveld refinement of **1c** was carried out as with **1a** and **1b**. The final agreement factors ($R_p = 0.084$, $R_{wp} = 0.109$) were slightly lower than the values obtained for **1b** and almost the same as for **1a**. Thus, the differences in experimental and calculated XRD pattern for the disordered model **1c** are comparable to those observed for the ordered structure type **1a**. The ranges and average bond distances and angles obtained for **1c** are: d(Si−O) = 1.531(9)−1.631(5) Å, $\bar{d}$(Si−O) = 1.605 Å; ∠(O−Si−O) = 84.3(3)−137.1(5)°, $\bar{\angle}$(O−Si−O) = 109.7°; ∠(Si−O−Si) = 142.5(7)−178.0(16)°, $\bar{\angle}$(Si−O−Si) = 152.5°.

The results of the Rietveld refinements of the SPXRD data show that all three structural models can be used to fit the experimental information within the limits of the techniques used. However, for reasons enumerated above, models **1a** and

(13) Thompson, P.; Cox, D. E.; Hastings, J. B. *J. Appl. Cryst.* **1987**, *20*, 79−83.

(14) McCusker, L. B. *Acta Crystallogr., Sect A* **1991**, *47*, 297−313.

(15) Lewis, Jr., J. E.; Freyhardt, C. C.; Davis, M. E. *J. Phys. Chem.* **1996**, *100*, 5039−5049.

(16) Weigel, S. J.; Gabriel, J.-C.; Puebla, E. G.; Bravo, A. M.; Henson, N. J.; Bull, L. M.; Cheetham, A. K. *J. Am. Chem. Soc.* **1996**, *118*, 2427−2435.

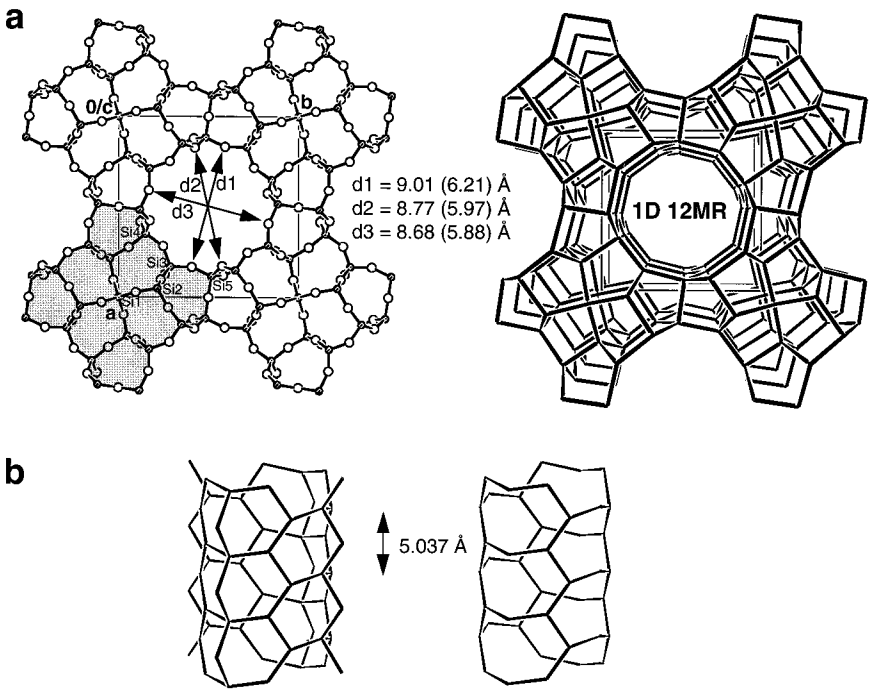

Figure 7. (a) Parallel projection of the structure (left) and perspective drawing of the topology (right) of calcined VPI-8 (**1a**), viewed down the [001] zone axis; values in parentheses denote approximate free pore diameters by substracting 2 $r_{vdW}(O) = 1.4$ Å. (b) 12MR channel with and without the slightly hidden T-atoms forming small 8MR "pockets" and showing the repeat unit of 5.037 Å along the channel direction, as viewed approximately parallel to *a*,*b* plane.

1c are slightly more appropriate. Note that when comparing **1a** and **1c** only one of seventeen Si atoms per unit cell is involved in the disorder (accounts for less than 3% of the total scattering intensity of the VPI-8 framework) and that the differences in the calculated XRD data created by the disorder are very small. The disorder is also not apparent in the ED data (see Figure 4). Simulations of ED patterns based on the disordered structure **1c** show no obvious streaking of the reflections spots. Thus, based on the data reported here, it is not possible to state whether VPI-8 contains a completely ordered structure (**1a**) or includes some slight disorder (**1c**).

Structural Features of VPI-8. It is interesting to note that the use of zinc in the synthesis of microporous materials has produced a number of new solids (VPI-7, VPI-8, VPI-9, VPI-10) that have not been produced synthetically using traditional aluminosilicate chemistry.[5,6] The original motivation for using zinc in the synthesis of microporous materials was to promote the formation of 3MRs in the resulting structures.[5] However, VPI-8 (Figure 7), which contains no 3MRs, is able to form only when zinc is present in the synthesis mixture.[5−7] Thus, the ability of zinc to promote 3MRs is just a partial view of a more general feature of zincosilicate crystal chemistry, the tendency to form small T−O−T angles.[17] This trend to form small T−O−T angles is observed in all of these new materials.

Figure 5b shows the very good agreement between the experimental HRTEM image (real-space averaged) and the simulated image of VPI-8 **1a**. The four adjacent 5MRs of the center of the new pinwheel structure building unit are clearly observed in both the experimental and simulated images along with the two 5MRs which are formed by connecting together two adjacent pinwheel centers. Therefore, we describe the VPI-8 structure via the use of a unit containing the four inner 5MRs plus the four outer 5MRs as the general structure forming pinwheel unit (shaded area in Figure 7a). The eight dark spots encircling the 12MR in the *a*,*b*-projection of HRTEM images correspond nicely to the eight pairs of slightly offset oxygen atoms (between two puckered atom layers parallel to the (110) plane) residing around the circumference of the 12MR channel, as illustrated in the unit cell model of Figure 5b. The increase of the projected atomic density in the region of the offset oxygen atoms results in the dark spots observed in the channel walls of the HRTEM image. Comprehension of the relationship between the structure and HRTEM image was critical in the understanding of the connectivity between the pinwheel building units and rationalizing the zigzag pattern of the 5MRs seen in the channel walls of the *a*,*b*-projection of VPI-8 (Figure 5b). Another important observation from the HRTEM image is the orientation of the pinwheel building units relative to the 12MR channels. As illustrated in the simulated HRTEM shown in Figure 5b, the sides of the seemingly square 12MR channel are not parallel to the unit cell axes. The formed 12MR channels (point symmetry 2) contain 6MRs of which only five T-atoms are exposed to the inner channel surface and one T-atom is slightly hidden in the channel walls (Figure 7b). The pore channels are basically built by four rows of bent 8MRs running parallel to the channel direction with a repeat unit of about 5 Å similar to the repeat unit found for other 1D 12MR channel systems, e.g., cancrinite (CAN) and ZSM-12 (MTW).[18] The slightly hidden T-site (Si2) divides each 8MR into a pair of 6MRs that have three T-atoms in common and thus form a small "pocket" within the channel walls.

Pore sizes for the 12MR channels were obtained by measuring ring diameters from O(center) to O(center). The pores of VPI-8 are not completely circular so three slightly different pore diameters (d1, d2, d3) measuring 9.01, 8.77, and 8.68 Å, respectively, are obtained (see Figure 7a). Assuming a van der Waals radius for oxygen of 1.40 Å, the corresponding free diameters of the pores can be calculated as 6.21, 5.97, and 5.88 Å, respectively, with an average value of 6.02 Å. The calculated values for the free pore diameter are consistent with the fact

(17) Camblor, M. A.; Davis, M. E. *J. Phys. Chem.* **1994**, *98*, 13151−13156.

(18) Meier, W. M.; Olson, D. H. *Atlas of Zeolite Structure Types*; Butterworth-Heinemann: Boston, 1992

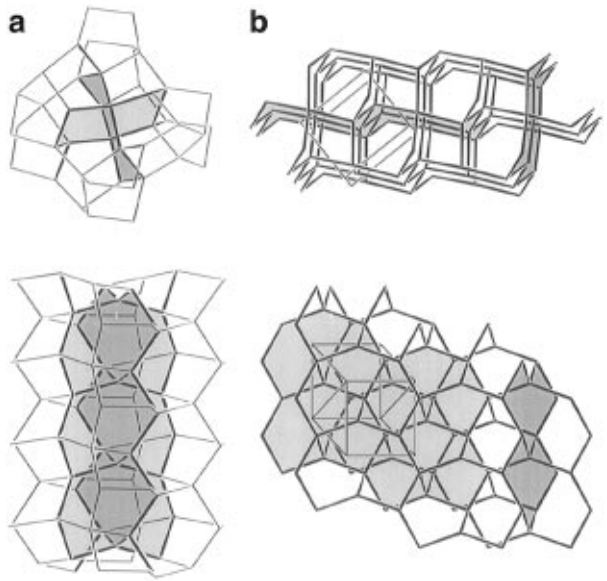

Figure 8. (a) Novel pinwheel structure building unit of VPI-8 with interlocking heart-shaped 8MRs (upper) and columns of heart-shaped rings formed by the stacking of the pinwheel building units (lower), the two perpendicular sets of 8MR hearts are shaded differently. (b) Section of the α-quartz structure built exclusively by two sets of nearly perpendicular layers of heart-shaped 8MRs, as seen parallel (upper) and perpendicular (lower) to the layers.

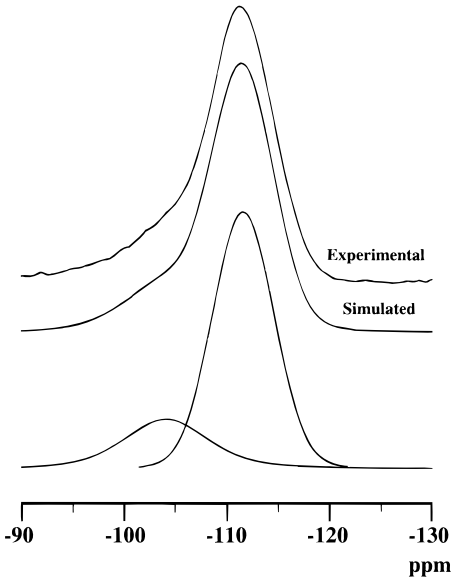

Figure 9. Solid-state ^{29}Si MAS−NMR spectrum of high-silica, calcined, acid-washed VPI-8.

that VPI-8 can adsorb 2,2-dimethylpropane which has a reported kinetic diameter of 6.2 Å.[12] Assuming an average free pore diameter of 6.02 Å and a cylindrical 12MR channel, a void volume of 152 Å^3/uc (0.08 cm^3/g) can be calculated. This calculated void volume approximately agrees with the void volumes measured by physical adsorption of nitrogen (0.1 cm^3/g) and cyclohexane (0.06 cm^3/g).[7] The slightly higher void volume obtained by nitrogen adsorption can be rationalized since a cylindrical channel shape was assumed with an average pore radius for the calculated void volume. Thus, some void volume accessible by the nitrogen probe molecules could be unaccounted for by the use of the assumption of a simplified pore shape. The slightly low void volumes predicted by the hydrocarbon probe molecules can be explained by incomplete packing of the hydrocarbon molecules in the pores of VPI-8.

As mentioned previously, the key to ascertaining the structure of VPI-8 was understanding the pinwheel structure building unit (shown in more detail in Figures 7 and 8 based on structure type **1a**). For this case, the pinwheel unit possesses point symmetry $\bar{4}$ with its symmetry axis only occupied by one type of crystallographically nonequivalent T-atom (Si1 = T1, see Figure 7a). This completely hidden T-site (with respect to the 12MR channel pores) reveals interesting characteristics, i.e., NMR behavior (*vide infra*). The main feature of the pinwheel building unit is the formation of interlocking heart-shaped 8MRs in the pinwheel center, as highlighted by thicker lines and shading in Figure 8a. By stacking several of these building units in a column, as occurs in the ordered structure types **1a** and **1b** of VPI-8, the heart-shaped 8MRs form two sets of 1D columns of hearts all pointing up or down, as can be seen from Figure 8a. The average plane of the slightly puckered 8MR hearts in one set is nearly perpendicular to the average plane defined by the 8MR hearts of the second set. When adjacent columns of pinwheel building units are related by translational symmetry, all heart-shaped 8MRs of one set point in the same direction and thus inversion centers within the unit cell are forbidden. As this arrangement of pinwheel units exists in the structure type **1a**, VPI-8 **1a** is an acentric structure as indicated by its space group, $P\bar{4}$. Structure type **1b** differs from VPI-8 **1a** in the relative orientation of the pinwheel building units (see Figure 6). Structure type **1a** contains pinwheel units that are all oriented identically. Thus, translational symmetry is achieved every ∼13 Å along the *a*- and *b*-axis, whereas in **1b**, every other column of pinwheel units are rotated 90° around the *a*-or *b*-axis. The resulting alternating pinwheel arrangement gives rise to the larger unit cell dimensions (a = b ≈ 18.5 Å) and different space group in **1b** (*vide supra*). The difference in the structure connectivity of **1a** and **1b** may be better seen in the relative orientation of the heart-shaped 8MRs in the pinwheel center. In **1a** all 8MR hearts of one set in different columns are pointing in the same direction, whereas in **1b** adjacent sets of heart columns point alternately up and down (see Figure 6). Note that each 8MR heart contains two T1-atoms that are related by translational symmetry along *c* and that a shift of ±1/2c of all T1-atoms within one pinwheel column causes the same change in the relative pinwheel orientation than the above mentioned 90° rotation.

To the best of our knowledge, the pinwheel structure building unit has never been observed in microporous materials before. However, the topology of the central part of this unit can be derived from the α-quartz structure,[19] as may be seen from Figure 8. α-Quartz is exclusively built of puckered layers that contain only the above mentioned, heart-shaped 8MRs (Figure 8b). There exist two sets of these layers that cross each other at an angle close to 90° forming parallel to the layers the same interlocked 8MR heart columns present in the center of the pinwheel unit of the VPI-8 structure (Figure 8a).

The calculated density of VPI-8 is 1.98 g/cm^3, assuming a fully connected pure silica framework, which is a typical density for high-silica, microporous materials.[20] The density values calculated from the structure correspond well to previously reported values determined by experimental methods.[7] A comparison of these values is as follows (calculated value (this work), experimental value[7]): density 1.98 g/cm^3, 1.90 g/cm^3, number of T-sites per unit cell 17 T/uc, 16.7 T/uc, framework density 19.8 T/1000 Å^3, 18 T/1000 Å^3.

NMR Studies. Figure 9 shows the ^{29}Si NMR spectrum of the sample of calcined high-silica (Si/Zn > 2000) VPI-8

(19) Kihara, K. *Eur. J. Mineral.* **1990**, *2*, 63−77
(20) Szostak, R. *Handbook of Molecular Sieves*; Van Nostrand Reinhold: New York, 1992.

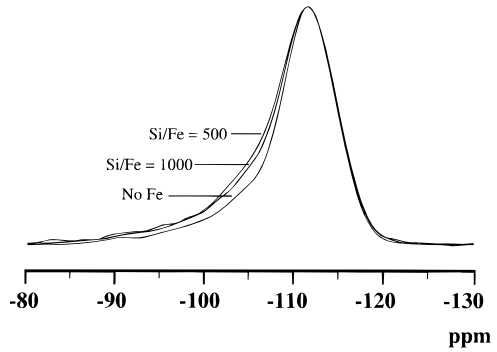

Figure 10. Solid-state ^{29}Si MAS−NMR spectra of high-silica, calcined VPI-8 prepared using no Fe, with $(Si/Fe)_{gel} = 500$ (VPI-$8_{Fe,1}$) and with $(Si/Fe)_{gel} = 1000$ (VPI-$8_{Fe,2}$).

obtained with a recycle delay of 300 s. This spectrum can be deconvoluted into two peaks at −105 and −112 ppm with relative intensities of 20% and 80%, respectively. In the proposed structure of VPI-8, T-atom sites T1 and T2 (see Figure 7) are situated further from the channel wall than the other T-sites. Given that the dominant contribution to the relaxation of ^{29}Si in zeolitic materials is due to interaction with paramagnetic dioxygen adsorbed in the pores,[21] it is speculated that T-sites T1 and T2 will have long relaxation times that may prevent the collection of quantitative ^{29}Si NMR spectra. In order to investigate the possibility that certain crystallographically distinct T-sites have longer relaxation times than others, samples of high-silica VPI-8 were prepared in which a small amount of Fe^{3+} [$(Si/Fe)_{gel} = 500-1000$] was included during synthesis. It is well-known that the presence of paramagnetic iron can significantly lower both ^{29}Si relaxation times, T_1 and T_2[22] [hereafter, relaxation times are given in italic letters to distinguish them from tetrahedral atom (T-atom) sites]. The amount of iron was kept low so as not to lead to the formation of amorphous iron silicates. Figure 10 shows a comparison of ^{29}Si NMR spectra for iron-containing [VPI-$8_{Fe,1}$: $(Si/Fe)_{gel} = 500$, VPI-$8_{Fe,2}$: $(Si/Fe)_{gel} = 1000$] and iron-free calcined VPI-8 obtained with recycle delay times of 10 s. Increasing the delay times to 300 s does not alter any of the spectra, indicating that the maximum obtainable signal intensities were achieved within a recycle delay time of 10 s. It is clear from the data shown in this figure that the addition of iron results in intensity enhancement of the spectra in the region between −90 to −105 ppm. For the sample where $(Si/Fe)_{gel} = 1000$ (VPI-$8_{Fe,2}$), no effect of the Fe^{3+} on the main resonance ca. −112 ppm is observed. However, for the case in which $(Si/Fe)_{gel} = 500$ (VPI-$8_{Fe,1}$), a slight broadening of all resonances is also observed and is attributable to the shortening of T_2 relaxation time due to paramagnetic iron. Thus, the difference observed in Figure 10 between the spectra of iron-free VPI-8 and VPI-$8_{Fe,2}$ is mainly due to a shorter T_1 for VPI-8 $_{Fe,2}$, while the difference between the spectra of VPI-$8_{Fe,1}$ and VPI-$8_{Fe,2}$ is attributable to the shorter T_2 for VPI-$8_{Fe,1}$. It should be noted that the relative enhancement of the spectrum in the region −90 to −105 ppm cannot be due to an impurity phase related to the introduction of iron in the synthesis. With $(Si/Fe)_{gel} = 500-1000$ and assuming that all of the iron is present as an iron silicate impurity, the population of the silicon in the impurity phase will be somewhere between 0.5 and 1% of the total silicon population (below NMR detection limits).

(21) Klinowski, J.; Carpenter, T. A.; Thomas, J. M. *J. Chem. Soc., Chem. Commun.* **1986**, 956.

(22) Engelhardt, G.; Michel, D. *High-Resolution Solid-State NMR of Silicates and Zeolites*; Wiley: Chichester, 1987.

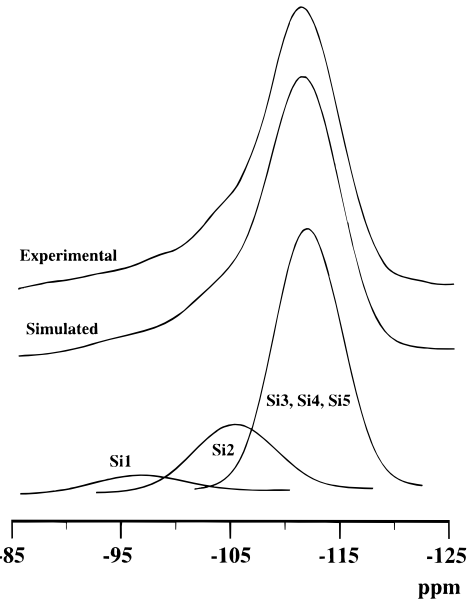

Figure 11. Experimental and simulated solid-state ^{29}Si MAS−NMR spectra of calcined, high-silica, iron containing VPI-$8_{Fe,2}$.

Contrary to the spectrum of iron-free VPI-8 (Figure 9), the spectra of iron-containing VPI-8 cannot be satisfactorily deconvoluted into two peaks. Figure 11 shows the ^{29}Si NMR spectrum of a calcined high-silica VPI-8 synthesized with a gel Si/Fe ratio of 1000 (VPI-$8_{Fe,2}$). Again, varying the recycle delay time from 10 to 300 s does not alter this spectrum. The spectrum is simulated using three Gaussian peaks at −97.5, −105.0, and −112.0 ppm with relative intensities of 6.0%, 23.6%, and 70.4%, respectively. The intensities of these peaks correspond roughly to 1/17, 4/17, and 12/17, respectively (consistent with T-site populations obtained from XRD data). It should be noted that the ^{29}Si NMR spectrum of the calcined VPI-8 for which $(Si/Fe)_{gel} = 500$ (VPI-$8_{Fe,1}$) can also be deconvoluted into three peaks with the same relative peak intensities as that obtained for the sample with $(Si/Fe)_{gel} = 1000$ (VPI-$8_{Fe,2}$). Furthermore, we note that the relatively broad NMR lineshapes for this material and the small intensity of the resonance ca. −97.5 ppm allows for a number of alternate deconvolutions for this spectrum where the relative intensity of the downfield peak varies from 5 to 8%. Thus, although the intensity ratios for the two resonances at −112 and −105 ppm are reliable and correspond to site populations implied from the structure solution, the relative intensity of the peak at −97.5 ppm should be interpreted with caution.

In light of the model for the structure of VPI-8 shown in Figure 7, the effect of iron in enhancing the resonances at −97.5 and −105 ppm (Figure 10) and the relative intensities of the three peaks in the NMR spectrum (Figure 11), the following assignment appears most reasonable: sites T3, T4, and T5 (of population 4 per unit cell each) are all readily accessible by dioxygen from the inside of the channel and therefore are not likely to have long relaxation times; these sites comprise the resonance at −112 ppm. Site T2 (of population 4 per unit cell) is in a different crystallographic environment and is also less accessible to dioxygen from the inside of the channel than T3, T4, and T5. This site is assigned to the resonance at −105 ppm. Finally, site T1 (of population 1/17), being "buried", is observed only in the presence of extra iron since it is not accessible to dioxygen molecules and is not likely to relax within the recycle times used (up to 300 s). This site is tentatively assigned to the resonance at −97.5 ppm. If this resonance is attributed to a Q^4 (Q^n stands for $X_{4-n}Si[OSi]_n$, X = OH or O^-)

Table 2. Proposed Large and Extra-Large Pore Structures Based on Novel Pinwheel Building Unit and Their Structural Characteristics

structure	T-sites in pore ring	space group (no.)	cell parameters [Å, deg]	unit cell content	density [g/cm^3]	FD[a] [T/1000 Å^3]	pore size [Å]
1a	12	$P\bar{4}$ (81)	$a = b = 13.053$ $c = 5.037$	$[Si_{17}O_{34}]$	1.976	19.8	6.0 × 6.0
1b	12	$P4_2/n$ (86)	$a = b = 18.461$ $c = 5.038$	$[Si_{34}O_{68}]$	1.976	19.8	6.0 × 6.0
2	14	$P2$ (3)	$a = 13.05$ $b = 10.10$, $\beta = 91.0$ $c = 15.90$	$[Si_{38}O_{76}]$	1.81	18.1	5.9 × 8.9
3	16	$P\bar{4}$ (81)	$a = b = 15.90$ $c = 10.10$	$[Si_{42}O_{84}]$	1.64	16.4	8.7 × 8.7
4	18	$C2$ (5)	$a = 31.80$ $b = 10.10$, $\beta = 91.0$ $c = 18.80$	$[Si_{92}O_{184}]$	1.52	15.2	9.0 × 11.7
5	20	$I\bar{4}$ (82)	$a = b = 26.60$ $c = 10.10$	$[Si_{100}O_{200}]$	1.40	14.0	11.9 × 11.9

[a] FD = framework density.

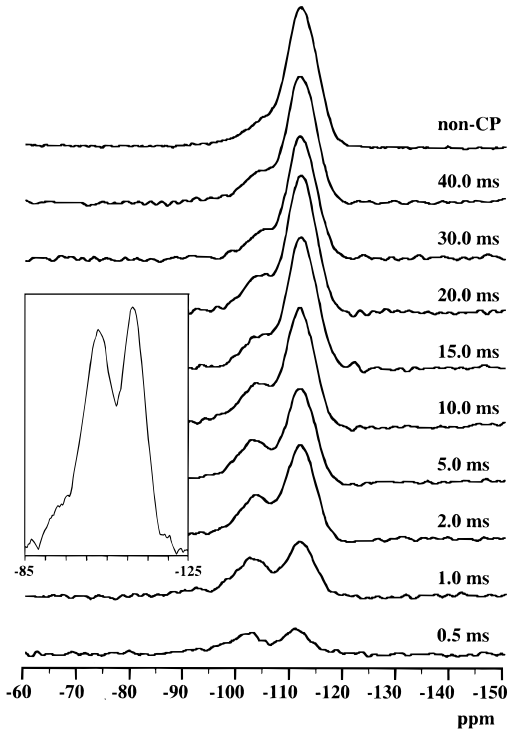

Figure 12. Variable contact time solid-state $^1H-^{29}Si$ CP/MAS−NMR spectra of high-silica, calcined, acid-washed VPI-8 loaded with cyclohexane. Inset shows magnified spectrum for CT = 1.0 ms.

silicon atom, then based on a number of correlations it is expected that this site will have a relatively small T−O−T bond angle of around 135° to 140° (see for example correlations given in ref 15 and 23). Although this is a rather small T−O−T bond angle for a high-silica molecular sieve, considering the novelty of the pinwheel unit and the absence of reliable bond angle information from the Rietveld refinement, the assignment of this resonance to a Q^4 site cannot be definitively ruled out.

The observed NMR intensity in the range −95 to −105 ppm could have contributions from silicons in silanol groups (Q^3) as well. To investigate this possibility, a sample of high-silica VPI-8 was prepared, calcined, and washed with HCl as mentioned in the Experimental Section. Cyclohexane was adsorbed in this sample in order to obtain $^1H-^{29}Si$ cross-polarization (between the protons of the organic and the silicon in the structure) spectra. Figure 12 shows a collection of such spectra obtained in the absolute intensity mode with contact times varying from 0.5 to 40 ms. The non-CP ^{29}Si NMR spectrum is also included for completeness. Three resonances are observed for all of these spectra, and since the resonance at ca. −95 ppm is low in intensity, a selected magnified spectrum is shown in the inset of Figure 12. By deconvoluting these spectra into three resonances and calculating the absolute areas of the peaks, it is clear that the peak at −95 ppm essentially reaches its full intensity at a contact time of 0.5 ms. Assuming that this peak corresponds to T1 and considering that the approximate distance between this site and the channel wall is ca. 5 Å, it is very unlikely that the cyclohexane protons can transfer magnetization to this site at such short contact times. Therefore, the enhancement of this peak can be attributed to silanol protons which have a shorter cross-relaxation time given an H−Si distance of ca. 2.5 Å. This is further confirmed by the observation that the unloaded sample also shows CP intensity for this resonance at short contact times. Thus, it can be concluded that at least some of the T1 sites in the structure of VPI-8 are not really Q^4, but rather Q^3 sites containing OH groups. The silanol group could be caused by the hydrolysis of a Si−O−Si connection with water (T1−O−T2 + H_2O ↔ T1−OH + T2−OH) and will allow considerable relaxation of the bond angles of the pinwheel unit. While this relaxation in the bond angle will tend to shift the resonance upfield, reducing the connectivity of this site from Q^4 to Q^3 will result in a downfield shift and can counteract the effect of increasing bond angle. Thus, the resonance at −97.5 ppm (Figure 11) can be attributed to either a Q^4 site with a small T−O−T bond angle, or a Q^3 site with a larger T−O−T bond angle, or a combination of both (the most likely scenario, *vide infra*). The latter interpretation is also consistent with the slight downfield shift of this peak in the CP experiment (inset Figure 12) and the broadness of this peak in the non-CP spectrum.

A similar analysis performed for the peak at −105 ppm (site T2) reveals that this resonance also has an initial growth rate much higher than the resonance at −112 ppm. Furthermore, the maximum signal intensity for this peak is not achieved until longer contact times (between 15 and 20 ms). Therefore, the initial enhancement of this peak at contact times of 0.5 and 1.0 ms can be attributed to the silanol protons while at longer contact times the cyclohexane protons can transfer magnetization to this site and thus allow it to achieve its maximum absolute intensity (contrary to T1, this site is somewhat accessible by cyclohexane inside the channel). Finally, the NMR resonances produced by sites T3, T4, and T5 being readily accessible by cyclohexane inside the channel grow slowly in intensity reaching their maximum absolute intensity at contact times around 10−15 ms.

(23) Engelhardt, G.; Radeglia, R. *Chem. Phys. Lett.* **1984**, *108*, 271−274.

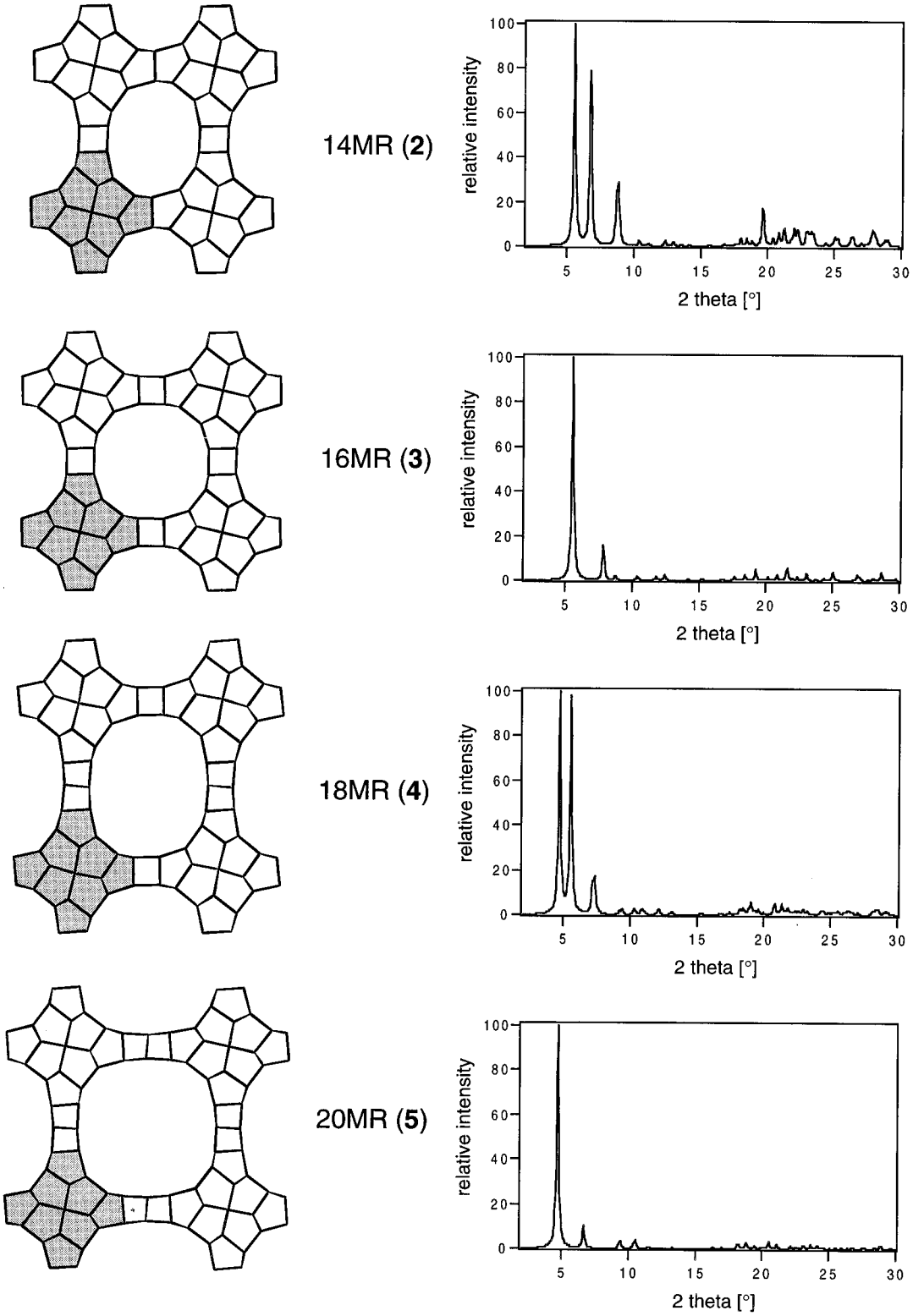

Figure 13. Hypothetical structures of theoretical extra-large pore analogues of VPI-8 **1a** based on the new pinwheel structure building unit with their corresponding, simulated PXRD patterns.

Based on the fast initial growth rates for the resonances at −95 and −105 ppm and the fact that these fast initial growth rates are attributable to cross-polarization from silanol protons, it can be concluded that at least a portion of the sites T1 and T2 are populated by silanol groups that could be the result of hydrolysis (T2 is the only T-site in the second coordination of T1). The hypothesis that at least some of the Si−O−Si bridges between T1 and T2 are hydrolyzed is also consistent with the results from the thermogravimetric analysis of high-silica, calcined, acid-washed VPI-8 which shows a weight loss of about 1% occurring at temperatures above 673 K. Furthermore, variable-temperature IR experiments of a calcined, acid-washed, high-silica sample of VPI-8 show a broad peak around 3680 cm^{-1} due to the presence of nonisolated Si−OH groups. This IR intensity disappears upon heating the sample to over 673 K (consistent with TGA results) and does not return until the sample is exposed to water at lower temperatures, i.e., room temperature. The presence of nonisolated Si−OH groups is also

consistent with observed and calculated SPXRD intensities not completely matching in the 15−25° 2θ range.

Hypothetical Structures Based on the Novel Pinwheel Building Unit. One of the most striking features of VPI-8 is the presence of the previously unobserved pinwheel building unit shown in Figure 8. This building unit seems to be uniquely suited for producing structures containing 1D channel systems comprised of 12 or more T-atoms. The minimum pore size that can be produced using four of these pinwheel units is a 12MR channel, which is found for VPI-8. Expanding the pore size by successive insertion of additional 4MRs in the channel walls seems theoretically quite feasible and leads to structure topologies shown in Figure 13. Structural characteristics of these hypothetical models with extra-large 1D channel systems containing 14MRs (**2**), 16MRs (**3**), 18MRs (**4**), and 20MRs (**5**) that are all based on the pinwheel structure building unit are presented in Table 2 and compared with the 12MR containing structure types **1a** and **1b** of VPI-8. In constructing the theoretical extra-large pore analogues of VPI-8, many different connectivities of the pinwheel building units were explored. The focus on acentric space groups (see Table 2) is emphasized since the space group of VPI-8 is most likely acentric (structure type **1a**). This emphasis leads to the maintenance of translational symmetry between adjacent columns of heart-shaped 8MRs and constant relative orientation of the pinwheel building units in each of the theoretical models as it is found for VPI-8 **1a**. Each of these frameworks gave reasonable DLS refinement results, and the PXRD patterns calculated from this analysis are shown in Figure 13. It is clear that the structural units found in VPI-8 are very appropriate for constructing extra-large pore frameworks that in particular do not violate known bonding and framework density constraints (see Table 2). It will be interesting to see if the zincosilicate chemistry used to prepare VPI-8 can be extended to synthesize extra-large pore materials.

Summary

The structure solution of the molecular sieve VPI-8 is achieved as a result of the synergistic combination of several characterization techniques. VPI-8 is an excellent candidate for investigation by HRTEM due to the 1D large pore channel system present in the structure. Extensive Rietveld refinement studies and HRTEM and solid-state NMR investigations were used to elucidate the topology of the VPI-8 structure and identify a novel molecular sieve building unit. The connection of four of these new pinwheel building units directly leads to a 12MR channel system, as found in VPI-8. By inserting 4MRs between the pinwheel building units, the formation of theoretical extra-large pore structures (>12MR) is possible.

Acknowledgment. The authors gratefully acknowledge Dr. John Higgins (Air Products) and Dr. James Kaduk (Amoco) for helpful discussions concerning the Rietveld refinement. The authors also acknowledge Dr. Michael Bennett for very helpful suggestions in the evaluation of the structural disorder. Dr. Hubert Koller and Dr. Larry Beck are acknowledged for numerous discussions regarding the interpretation of the NMR spectra. The SPXRD data were collected at the X7A beam line, National Synchrotron Light Source, Brookhaven National Laboratory, which is supported by the Department of Energy, Division of Material Sciences and Division of Chemical Sciences. We also wish to thank Ron Medrud (Chevron) for collecting the synchrotron data. HRTEM work was carried out at the Center for High Resolution Electron Microscopy at Arizona State University. Dr. Ming Pan acknowledges the support of the HREM Industrial Associates Program at Arizona State University.

Supporting Information Available: Atomic coordinates and interatomic distances and profiles for SPXRD patterns (12 pages). See any current masthead page for ordering and Internet access insturctions.

JA954337Q